Transient interactions studied by NMR : iron sulfur proteins and their interaction partners

Xu, X.

Dynamics in a Pure Encounter Complex of Two Proteins Studied by Solution Scattering and Paramagnetic NMR spectroscopy

Xu X, Reinle W, Hannemann F, Konarev PV, Svergun DI, Bernhardt R, and Ubbink M. *JACS*. 2008, 130, 6395-5403.

Abstract

In the general view of protein complex formation, a transient and dynamic encounter complex proceeds to form a more stable, well-defined and active form. In weak protein complexes, however, the encounter state can represent a significant population of the complex. The redox proteins adrenodoxin (Adx) and cytochrome *c* (C*c*) associate to form such a weak and short-lived complex, which is nevertheless active in electron transfer. To study the conformational freedom within the protein complex, the native complex has been compared to a cross-linked counterpart, using solution scattering and NMR spectroscopy. Oligomerization behavior of the native complex in solution revealed by small-angle X-ray scattering indicates a stochastic nature of complex formation. For the cross-linked complex interprotein paramagnetic effects are observed, while for the native complex extensive averaging occurs, consistent with multiple orientations of the proteins within the complex. Simulations show that cytochrome *c* samples about half of the surface area of adrenodoxin. It is concluded that the complex of Adx/C*c* is entirely dynamic and can be considered as a pure encounter complex.

Introduction

The formation of a protein complex is at least a two-step process, in which a dynamic encounter complex precedes the final, well-defined complex. It has been proposed that the role of the former is to enable a reduced-dimensionality search of the optimal binding geometry, thus accelerating molecular association[1]. Generally, it is assumed that the encounter state exists only briefly and leads quickly to the well-defined, final complex. However, analysis by NMR spectroscopy has suggested that for weak protein complexes the encounter state represents a significant fraction of the population or can even be the dominant form. This was concluded from the observation that for these complexes, the average chemical shift perturbations observed upon complex formation are very small and the residues involved are spread over a large part of the protein surface.[2,3] This view is in line with the conclusions of independent studies on the electron transfer rates in electron transfer (ET) complexes [4,5]. Recently, the encounter state was visualized by a paramagnetic NMR technique for complexes in which it represents a small fraction of the population [6,7]. In weak protein complexes the fraction of time spent in the encounter complex may be largest, because a balance between specificity and fast dissociation has to be found.

To study the elusive encounter state and obtain more direct evidence of its dynamic nature, we decided to compare an electron transfer complex in its 'native' form with a cross-linked (CL) complex of the same proteins. Adrenodoxin (Adx) is a 14.4 kDa protein that belongs to the family of vertebrate-type 2Fe-2S ferredoxin. It is involved in steroid hormone biosynthesis by acting as an electron shuttle between NADPH-dependent adrenodoxin reductase and several cytochromes P450[8]. *In vitro* electron transfer from adrenodoxin reductase to Adx is often monitored by fast subsequent electron

transfer from Adx to mitochondrial cytochrome *c* (C*c*). C*c* serves in the reaction as a model for cytochrome P450[9]. The interaction of yeast C*c* with full length bovine Adx and truncated Adx4-108 has been studied by NMR spectroscopy [3]. It was shown that a complex is formed despite the fact that the proteins are non-physiological partners. The dissociation constant is 25 μM in 20 mM potassium phosphate buffer, which is in the range of other electron transfer complexes [10]. Chemical shift mapping indicated that an extensive interface exists in this complex, especially on the Adx part. The results suggested that this complex is a dynamic ensemble of orientations with both proteins sampling other surface areas, away from the predominant binding sites. Thus, the complex potentially represents a good model to study the characteristics of encounter complex. The FeS cluster in Adx and the heme in C*c* can serve as natural paramagnetic centers, to probe the averaging effects within the complex.

In this study, a CL complex was constructed with an engineered intermolecular disulfide bond to serve as a rigid control complex. Small Angle X-ray Scattering reveals an oligomerization behavior different for the CL and native complexes, consistent with dynamic complex formation. It is shown that for the rigid complex large chemical shift perturbations and significant intermolecular paramagnetic effects can be detected, in contrast with the native complex. These differences are explained by averaging effects due to multiple orientations of two proteins in the native complex. Simulations suggest that in the native complex averaging over a surprisingly large interaction interface is required to reduce the paramagnetic effects to insignificant values, which is consistent with the observations from NMR chemical shift mapping. The results indicate that this complex is entirely dynamic and can be interpreted as a pure encounter complex.

Materials and Methods

Site-directed mutagenesis experiment and protein production

Site directed mutagenesis was performed using the QuikChange method (Stratagene, La Jolla, CA). Two mutants, yeast C*c*V28C and the double mutant L80C/C95S of truncated, bovine Adx (residues 4-108)[11] were constructed. The C95S mutation removes a native semi-exposed Cys. Mutations were confirmed by DNA sequencing. Production and purification of wt and mutant C*c* were performed as reported [12].

^{15}N enrichment of CcV28C and CL complex

A colony of freshly transformed *E. coli* (BL21) was used to inoculate 3 mL LB medium supplemented with 100 mg/L ampicilin. The preculture was incubated at 37° C, 250 rpm until turbidity. One liter of M9 minimal media in a 2 L Erlenmeyer flask was inoculated with one mL of preculture and incubated at 37° C, 200 rpm for 36-38 hours. For isotope enrichment, either ^{15}N-labeled C*c*V28C or ^{15}N-labeled AdxL80C and the unlabeled partner protein were used in the cross-linking procedures. The production and expression of Adx mutant was performed as reported[3] and purified using a Source-30Q anion exchange column and a Superdex® G75 gel filtration column.

Cross-linking

C*c*V28C and AdxL80C were treated with 5 mM DTT in 50 mM sodium phosphate buffer pH 6.5 with 500 mM Na_2SO_4. After 1 hour, the buffer was changed to 50 mM Tris pH 8.0 containing 500 mM Na_2SO_4 using ultrafiltration on a 3 kDa cutoff membrane. Both proteins were diluted to 200 μM, mixed and $K_3Fe(CN)_6$ was added to the final concentration of 5 mM to oxidize the mixture. The covalent complex was purified from the C*c*V28C and AdxL80C monomers and homodimers by ion exchange chromatography. The buffer of the oxidized mixture was changed to 50 mM Tris pH 8.0 and a small amount of ascorbic acid

was added to reduce the C*c* of the heterodimer, before the mixture was loaded to a MonoQ column attached to an ÄKTA® FPLC system (GE Healthcare Inc, Benelux). The buffer was then replaced by ultrafiltration. The C*c*V28C monomer and homodimer were found in the flow-through. The heterodimer was eluted with a salt gradient ranging from 150 mM to 200 mM NaCl, while AdxL80C was not eluted until the salt concentration was increased to 400 mM. The CL heterodimer was characterized on an analytical Superdex® G75 10/300 GL gel filtration column using a solution containing 25 mM sodium phosphate pH 7.4. For preparation of the reduced CL complex, 1 equivalent of ascorbic acid was added to reduce C*c*. For preparation of the oxidized CL complex, excess $K_3Fe(CN)_6$ was added and then removed by buffer exchange with phosphate buffer, which had been pretreated with Chelex 100 (Sigma, St. Louis, MO).

Small Angle X-ray scattering

The synchrotron radiation X-ray scattering data were collected on the X33 camera of the EMBL (DESY, Hamburg, Germany)[13] and analyzed following standard procedures [14]. Solutions of native and cross-linked complex of C*c* and Adx were measured at 15°C in solute concentration range from 2.4 to 24.0 mg/ml in 10 mM Hepes, pH 7.4 buffers with 0, 40, 80, 120, 200 and 300 mM NaCl. The solutions of native complex of solute range from 2.4 to7.2 mg/ml in 20 mM potassium phosphate buffer were also measured to check the oligomerization status. The data were recorded using a MAR345 two-dimensional image plate detector at a sample-detector distance of 2.7 m and a wavelength of $\lambda = 1.5$ Å, covering the range of momentum transfer $0.012 < s < 0.45$ Å^{-1} ($s = 4\pi \sin\theta/\lambda$, where 2θ is the scattering angle). All data manipulations were performed using the program package PRIMUS.[15] The forward scattering *I(0)* and the radius of gyration (R_g) were evaluated using the Guinier

approximation assuming that at very small angles ($s < 1.3/R_g$) the intensity is represented as $I(s) = I(0) \exp(-(sR_g)^2/3)$. These parameters, and the maximum diameter D_{max} of the particle were also computed from the entire scattering patterns using program GNOM.[16] The excluded volume V_p of the particle was computed from the Porod invariant.[17] The molecular masses of the solutes were evaluated by comparison of the forward scattering with that from reference solutions of bovine serum albumin (MM = 66 kDa) The low resolution shapes were reconstructed *ab initio* by DAMMIN,[18] the scattering from the high resolution models was computed by CRYSOL[19] and the volume fractions of oligomers were determined by OLIGOMER [15].

The structure of the C*c*/Adx cross-linked complex was refined by rigid body modeling using the program SASREF.[20] The latter program employs a simulated annealing (SA) protocol to generate an interconnected assembly of subunits without steric clashes fitting the scattering data. Contact information on the residues involved in the dimerization was included as a restraint. The scattering amplitudes from the crystallographic models of C*c* (PDB 2YCC)[21] and Adx (PDB 1AYF) [22] were calculated using the program CRYSOL[19].

For a quantitative description C*c*/Adx native complex at different protein and NaCl concentrations the experimental intensity $I_{exp}(s)$ was represented by linear combinations of the curves computed from putative complexes at different stoichiometry. Given the scattering curves of such components, program OLIGOMER [15] finds the volume fractions by solving a system of linear equations to minimize discrepancy between the experimental and calculated scattering curves

$$\chi^2 = \frac{1}{N-1}\sum_j \left[\frac{I(s_j) - cI_{calc}(s_j)}{\sigma(s_j)}\right]^2 \qquad (2.1)$$

where N is the number of experimental points, c is a scaling factor and $I_{calc}(s)$

and $\sigma(s_j)$ are the calculated intensity and the experimental error at the momentum transfer s_j, respectively. The possible components included individual proteins ("monomers"), 1:1 cytochrome/adrenodoxin complex ("dimer"), and tentative higher oligomeric models, 2:1 and 1:2 complexes ("trimers") and 2:2 complexes ("tetramers").

NMR experiments

NMR experiments were performed in 20 mM phosphate buffers, pH 7.4, consistent with earlier work. In this buffer, no indications for oligomerization of the complex were observed as based on the absence of concentration-dependent line broadening effects. In 10 mM Hepes pH 7.4, the NMR spectra of the complex exhibited very broad line width, consistent with trimer and tetramer formation as observed in the SAXS experiments. Samples contained 0.2 mM to 1 mM (for assignment) protein, 5% D_2O. For backbone assignment of CL complex, 0.4 M Na_2SO_4 was present in the buffer. Protein concentrations were determined using ε_{410} = 106 $mM^{-1}cm^{-1}$ for ferric C*c*, ε_{550} = 27.5 $mM^{-1}cm^{-1}$ for ferrous C*c*, ε_{414} = 9.8 $mM^{-1}cm^{-1}$ for oxidized Adx, and ε_{550} = 31.7 $mM^{-1}cm^{-1}$ for the reduced CL heterodimer.

All NMR experiments were carried out on a Bruker DMX 600 spectrometer equipped with a TXI-Z-GRAD probe or a TCI-Z-GRAD cryoprobe. For ^{15}N-labeled C*c*V28C, the assignment of backbone amide resonances was based on WT C*c* [23] and confirmed by the analysis of an ^{15}N NOESY-HSQC spectrum. The backbone amide assignment of AdxL80C was completed with ^{15}N TOCSY-HSQC and NOESY-HSQC spectra based on previous assignments for Adx [3]. For the CL heterodimer, a ^{15}N NOESY-HSQC spectrum was recorded at a temperature of 301 K. The backbone amide assignments were confirmed by the analysis of NOE connectivities. Processing was performed using AZARA (http://www.bio.cam.ac.uk/pub/azara) and the spectra were analyzed in Ansig-for-Windows [24]. The averaged amide chemical shift perturbation ($\Delta\delta_{avg}$) was

derived from

$$\Delta\delta_{avg} = \sqrt{\frac{(\Delta\delta \mathrm{N}/5)^2 + \Delta\delta \mathrm{H}^2}{2}} \qquad (2.2)$$

where $\Delta\delta$N represents the chemical shift change for the amide nitrogen and $\Delta\delta$H represents the chemical shift change for the amide proton.

PCS measurements and R_1 relaxation rate measurements

For free C*c*V28C, the chemical shift difference between ferric and ferrous C*c* was taken to represent the PCS. To detect PCS in the native complex, two HSQC spectra were recorded for ^{15}N Adx (0.2 mM) in the presence of ferric or ferrous C*c* in a ratio 1:2.5. For the CL complex, four samples were prepared, with either C*c* or Adx labelled with ^{15}N and with C*c* either reduced or oxidized. Thus, PCS could be measured for both C*c* and Adx within the complex. Magnetic susceptibility tensors were calculated according to Worrall *et al.*[23]. The tensor size and orientation are identical within error for free C*c* and the CL heterodimer and similar to those reported [23].

The longitudinal relaxation rates of the amide protons of C*c* in the free state and the native and CL complexes were obtained by a series of inversion recovery (IR) ^{1}H-^{15}N HSQC spectra. Water suppression was achieved by presaturation. The IR relaxation delays (τ) were 0.001, 0.01, 0.03, 0.05, 0.1, 0.2, 0.35, 0.55, 0.85, 1.4 and 3.0 s. The spectra were acquired in an interleaved way, such that all delays were applied before incrementing the indirect dimension. The amide proton R_1 relaxation rates were obtained by a three parameter single-exponential fit of the HSQC cross-peak intensities $I(\tau)$ using

$$I(\tau) = I_{eq} - (I_{eq} - I_0)\exp(-R_1\tau) \qquad (2.3)$$

where I_0 is the magnetization at time τ =0 s and I_{eq} is the equilibrium magnetization. $I(\tau)$ and τ are the dependent and independent variables, respectively and I_0, I_{eq} and R_1 are the fitted parameters.

Site-specific spin labeling

C*c*V28C was incubated with 10 mM DTT in 0.1 M Tris·HCl (pH 8.0)/0.1 M NaCl for 2 h at room temperature to reduce intermolecular disulfide bonds. DTT was removed by passing the protein solution through a PD-10 column (Amersham Pharmacia, Uppsala, Sweden). The resulting monomeric protein was reacted with 10-fold excess of paramagnetic label [MTSL, (1-oxyl-2,2,5,5-tetramethyl-3-pyrroline-3-methyl)-methanethiosulfonate] or diamagnetic control label [MTS, (1-acetyl-2,2,5,5-tetramethyl-3-pyrroline-3-methyl)-methanethiosulfonate] and incubated overnight at room temperature. MTSL and MTS were purchased from Toronto Research Chemicals (North York, ON, Canada) and used without further purification. Upon completion of the reaction, the solution was passed through a PD-10 column to remove any unreacted label, and the buffer was changed by ultrafiltration. The yield of labeling was about 90% as estimated from double-integrated EPR spectra of C*c*-MTSL and a control sample containing a known amount of free MTSL. Samples of ^{15}N Adx complexed with either C*c*V28C-MTSL (1:2.5) or C*c*V28C-MTS were prepared in a parallel way. Both samples contained the same amount of ^{15}N acetemide as an internal reference. HSQC spectra were measured for both samples and the attenuation factor was determined by taking the ratio of heights of crosspeaks observed for amide resonances of Adx for both samples (I_{para}/I_{dia}). The PRE ($R_{2,para}$) was calculated from the following equation

$$\frac{I_{para}}{I_{dia}} = \frac{R_{2,\,dia}\exp(-tR_{2,\,para})}{R_{2,\,dia} + R_{2,\,para}} \qquad (2.4)$$

Where t is the INEPT evolution time of HSQC (9 ms) and $R_{2,dia}$, the diamagnetic transverse relaxation rate was obtained from the line width of the HSQC crosspeaks of the ^{15}N Adx in the complex with C*c*V28C-MTS, following the reported method [25].

To exclude the possible contribution of PRE due to the non-specific interaction between MTSL nitroxide group with Adx, we also estimated the PRE effect caused by several concentrations of free nitoxide spin label TEMPOL. Only at very high concentration of free spin label TEMPOL (> 10 mM), a general broadening effect is found for Adx, which is consistent with previous studies.[26,27] At 0.5 mM, the concentration of labeled protein used in our experiments, PRE contributions due to non-specific interactions are < 5 s^{-1}.

Structure calculation of the CL complex

The structure coordinates were taken from Protein Data Bank, PDB entries 1YCC[28] for C*c* and 1AYF for Adx.[22] The mutations were introduced in Swiss-Pdb viewer.[29] The protein structure coordinates were linked together through a disulfide bond formed by C28 of C*c* and C80 of Adx in XPLOR-NIH.[30] By consecutive rotation of the five torsion angles between C*c*V28C C_α and AdxL80C C_α in steps of 10°, the conformation space was sampled systematically and the rotamers were scored on the basis of van der Waals, PCS and PRE energy terms. The tensor and the twenty intermolecular PCS observed for Adx were used as input in the structure calculations. From the previous amide proton R_1 measurement of free Adx, it was found that PRE is insignificant when the atom is more than 16 Å away from the 2Fe-2S cluster.[31] Therefore, the intermolecular PREs observed for C*c* residues were converted to loose distance restraints (10-20 Å). One hundred structures with lowest energies were selected for further refinement. In the last refinement stage, the extra energy term defining the geometry of disulfide bond [32] was added. The final ensemble of the ten best structures and restraints used for structure modeling have been

submitted to the PDB, entry 2JQR.

PCS simulations

The structure coordinates of C*c* (PDB entry 1YCC) and Adx (PDB entry 1AYF) were used for PCS simulations. The relative diffusional movement of the proteins in the native complex was decomposed into two types of rotations. One is the rotation of Adx around its own center of mass (wobbling motion) and the other is the rotation of Adx around the C*c*, resulting in the translational movement over its surface. It should be noted that from the point of view of Adx, the former can be considered as rotation of C*c* around Adx and the second as wobbling of C*c*. For the convenience of calculation, the heme metal center of C*c* was used as the rotating center for the second movement. Pseudoatoms representing the magnetic susceptibility tensor were used as the reference frame. Each rotation can be further decomposed into the rotations around the X, Y and Z axes. Six angle variables are thus used to describe the rotation range. The initial orientation of two proteins was generated in a way that N16 of C*c* is in close contact with L80 of Adx. The initial distance of two rotating centers was set to be 29 Å. This brings the proteins together in an orientation with the centers of the CSP affected areas at close distance. Then the effect of averaging over the six rotating and wobbling axes was evaluated by generating 40-200 orientations randomly within a given angle range. If the rotation caused the structures in a certain orientation to be either clashing or not touching, the distance was increased (decreased) until both proteins were just in contact. The averaged intermolecular PCSs were calculated for amide protons of Adx in this ensemble and compared to the PCSs predicted for the starting structure. The significance cutoff of proton PCS was set to be 0.025 ppm. The rotations of Adx around C*c*, in the direction that changes the angle between Adx and the heme plane (θ) leads to most averaging of the PCS. On the other hand, rotations of Adx around its centre of mass (wobbling) have a smaller effect. The chemical shift perturbation

map of C*c* shows effects mostly at the front face[3] around the heme edge, implying that the angle range for Adx rotation is small. It was estimated to be at most θ = 75°. The angles for Adx wobbling need to be at least 100-120° to reduce the PCS to below the detection limit.

Results

Heterodimer formed by CcV28C and AdxL80C

To study the degree of dynamics in the complex of C*c* and Adx, a comparison was made between the native complex and a CL counterpart. The proteins were cross-linked using a disulfide bridge between engineered cysteine residues on C*c* (V28C) and the truncated form of Adx (residues 4-108)[22] (L80C) (in the following text, Adx refers to Adx4-108). The cysteine mutants were designed based on previous chemical shift mapping data[3] such that they are exposed on the surfaces and close to the predominant interaction interface. The CL complex does not necessarily mimic the electron transfer active form, but should represent a well-defined complex that is much less mobile than the native complex. Cross-linking experiments show that C*c*V28C and AdxL80C mutants can be linked by a disulfide bond with the best yield (20-30%) under high ionic strength conditions. The cross-linked products were separated using ion exchange chromatography. Analytical gel filtration shows that the engineered heterodimer has a molecular weight about 20-30 kDa (expected 23.5 kDa). The heterodimer of ^{15}N-C*c*V28C and AdxL80C was also characterized by mass spectrometry, which confirmed the formation of the heterodimer.

Small-angle X-ray scattering (SAXS)

SAXS was employed to analyze the oligomeric composition of C*c*/Adx

complexes in solution. In 10 mM Hepes buffer pH 7.4, the overall parameters of the CL complex in Table 1 indicate that it remains heterodimeric at all solute concentrations, independent of the presence of NaCl. The low resolution shapes of the complex reconstructed from the SAXS data *ab initio* and by rigid body analysis (Figure 1.1A) match the NMR-predicted model (see below, structural modeling of CL complex). The native complex demonstrates a completely different behavior, strongly depending on the solute concentration and ionic strength in 10 mM Hepes buffer. The experimental curve at 200 mM NaCl can be fitted well by the computed scattering from a mixture of C*c* and Adx, indicating that the native complex is an electrostatic complex and dissociates at higher NaCl concentrations. A reduction in salt concentration promotes formation of dimeric species but also higher oligomers are observed. In salt-free solutions with low protein concentration (2.4 mg/ml), the overall parameters are close to those of a heterodimeric complex (Table 2.1). The size of the complex grows with protein concentration (Table 2.1) and at 24 mg/ml the solute is largely tetrameric, as also revealed by *ab initio* and rigid body models displaying side-by-side dimers (Figure 2.1B). To obtain quantitative estimates of the equilibrium, the data were fitted allowing for mixtures of different oligomers of C*c* and Adx. The analysis included monomers, heterodimers, tetramers but also tentative trimers built by removing one monomer from the tetramer, and these mixtures indeed provided good fits to the experimental data at different solute concentrations (Figure 2.2, curves (1-4)). Strikingly, a significant proportion of trimeric species was detected for all concentrations, and attempts to fit the data without trimers significantly worsened the fits (Table 2.1). The formation of tetramers is thus proceeding via trimers and not by association of two heterodimers. The latter association would have been expected for the case of specific dimerization and teteramerization, whereas the actually observed oligomerization suggests a stochastic encounter complex formation. This finding is further corroborated by the fact that the CL heterodimer does not form

tetramers even at high solute concentrations. Apparently the CL heterodimers lack the mobility in solution necessary for the effective formation of interdomain links *via* an encounter mechanism. In 20 mM potassium phosphate pH 7.4, which is the buffer used in previous and current NMR experiments, the SAXS data indicate that the data for the native complex at 2.4 mg/ml can be well fitted with a 1:1 complex (Figure 2.2, curve (5), χ=1.41) or a mixture of monomers and 1:1 complex (χ=1.26), in the latter case the volume fraction of monomeric species does not exceed 40%. At high protein concentration and a 2:1 ratio Cc:Adx, the curve can be fitted with a 1:1 (χ=1.52) or a mixture of 1:1 and 2:1 complexes (χ=1.15). These results indicate that the presence of 20 mM phosphate buffer largely precludes oligomerization of the complex.

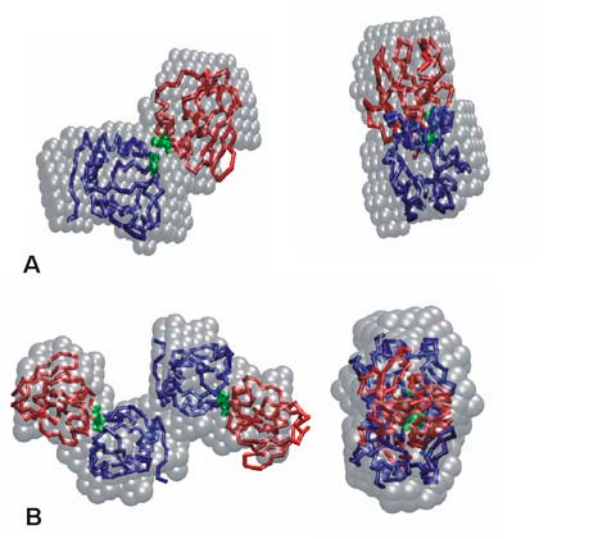

Figure 2.1. *Ab initio* bead model of CL complex and native tetramer model obtained from SAXS data.

A. *Ab initio* bead model of CL complex obtained by DAMMIN (gray semi-transparent spheres) superimposed with the rigid body model of the heterodimer constructed by SASREF. The cytochrome *c* and adrenodoxin models are displayed as blue and red C_α traces, respectively. Residues Val28 of C*c* and Leu80 of Adx are indicated by green spheres. The right view is rotated counter-clockwise around the vertical axis.

B. *Ab initio* bead model of native complex at high concentration in salt-free buffer superimposed with the heterotetramer constructed by rigid body refinement. The representations and color codes are as in A.

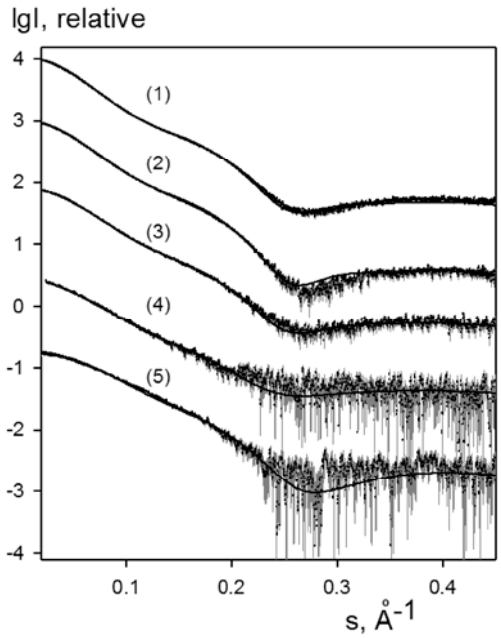

Figure 2.2. SAXS data from native C*c*/Adx complex in salt-free solutions (curves (1)-(4) correspond to solute concentrations 24, 12, 6 and 2.4 mg/ml in 10 mM Hepes buffer pH 7.4, respectively, curve (5) is from 2.4 mg/ml in 20 mM potassium phosphate pH 7.4 buffer). Dots with error bars: experimental data, solid lines: best fits by OLIGOMER from mixtures of monomers, heterodimers, trimers and tetramers with volume fractions in Table 1 (for curves (1-4)). For curve (5) the best fit comes from 1:1 complex. The intensities are displayed as functions of momentum transfer $s = 4\pi \sin\theta/\lambda$, where 2θ is the scattering angle and λ=1.5 Å is the X-ray wavelength, and successive curves are displaced down by one logarithmic unit for clarity.

Table 2.1 Parameters of native Cc/Adx complex from SAXS data.

Native complex, in 10 mM Hepes, pH 7.4					*CL complex*	*Cc/Adx (NMR)*
c, mg/ml	**24**	**12**	**6**	**2.4**	**3-12**	**-**
R_g, Å	28.3±0.7	28.3±0.7	26.5±0.5	24.4±0.7	21.4±0.5	20.4
D_{max}, Å	90±5	90±5	90±5	80±5	80±5	70
V_p, 10^3 Å^3	63±6	52±5	43±5	35±4	42±5	45
MM, kDa	44±5	42±5	35±4	25±4	22±3	24.3
χ^{MDT}	2.45	1.72	1.56	1.25	-	-
χ^{MTT}	1.84	1.47	1.41	1.17	-	-
χ^{MDTT}	1.84	1.43	1.35	1.15	1.45	-
$V_{mon,\%}$	0	0	6±5	24±5	0	-
$V_{dim,\%}$	0	8±5	25±5	24±5	100	-
$V_{tri,\%}$	48±5	47±5	54±5	52±5	0	-
$V_{tet,\%}$	52±5	45±5	15±5	0	0	-

Notations: R_g, radius of gyration; D_{max}, maximum size, V_p, excluded volume of the hydr particle, MM, molecular mass of the solute, χ denote discrepancy between the expetim data and best fits from mixtures: χ^{MDT} monomers/dimers/tetramers, monomers/trimers/tetramers and χ^{MDTT} monomers/dimers/trimers/tetramers, V_{mon}, V_{dim} and V_{tetr} are the volume fractions of the oligomeric species for the latter fits. The right column gives the values computed from the NMR model.

Chemical shift perturbations

Complex formation leads to changes of the chemical environment of residues in the interface, due to solvation changes and physical interactions with the partner proteins. The resulting chemical shift perturbations can be used to identify the residues involved in binding. Previously, we reported such chemical shift perturbations for the formation of the native 1:1 complex of C*c* and Adx in 20 mM phosphate buffer [(3)]. For C*c*, the maximum chemical shift change ($\Delta\delta_{avg}$) is only 0.08 ppm and for Adx, the chemical shift changes are even smaller ($\leq$ 0.04 ppm). According to the perturbations, dominant binding site in C*c* is around the heme edge, while for Adx the effects are spread over an extensive area (Figure 2.3). Under the same NMR experimental conditions, the CL complex shows perturbations with larger $\Delta\delta_{avg}$ values, of up to 0.35 and 0.27 ppm for C*c* and Adx, respectively, and the residues involved are localized to the area around the site of cross-linking (Figure 2.3). It was proposed that in the native complex C*c* may sample large surface area of Adx and multiple orientations are in fast exchange. The comparison of NMR chemical shift perturbation data for native and CL complex suggests that due to the disulfide bonding, reduced mobility in the single orientation CL complex leads to a more localized interface and larger chemical shift perturbations.

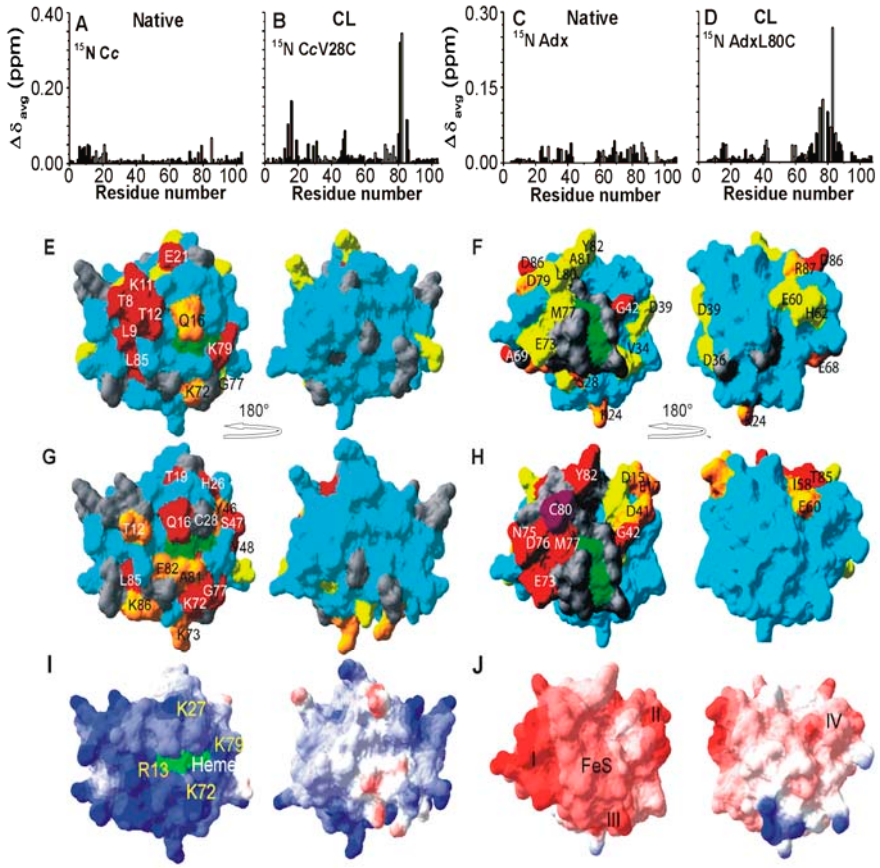

Figure 2.3. Chemical shift perturbations of native and CL complexes and the comparison with the electrostatic potential of C*c* and Adx

A-D) $\Delta\delta_{avg}$ for observed residues of C*c* (A, B) and Adx (C, D) for the native (A, C) and CL complex (B, D). CSP for the native complex were taken from literature (3). (E-H) surface representations of C*c* (E, G) and Adx (F. H) showing the CSP for native (E, F) and CL complex (G, H). Residues are colored in red, orange, yellow, and blue according to the $\Delta\delta_{avg}$ categories ($\geq$0.04, $\geq$0.03, $\geq$0.02 and <0.02 ppm). Residues without assignment are in gray and iron sulfur binding loop and heme group are in green. (I, J) surface representation of the electrostatic potential of C*c* (I) and Adx (J), important charged residues (R13, K27, K72, K79 of C*c*) or patches involoved (I, II, III, IV of Adx) in the interaction are labeled.

Intermolecular paramagnetic relaxation enhancement

The FeS cluster in Adx is paramagnetic, causing increased relaxation and thus line broadening of the NMR resonances of nearby nuclei due to a dipolar interaction with the unpaired electrons. Not only residues of Adx are affected, also C*c* residues that get sufficiently close to the FeS cluster should experience such effects. These intermolecular paramagnetic effects should affect the transverse relaxation rates (R_2) of the protons most strongly. However, transverse relaxation is also very sensitive to the increase of the tumbling time of C*c* upon complex formation as well as exchange broadening. No diamagnetic

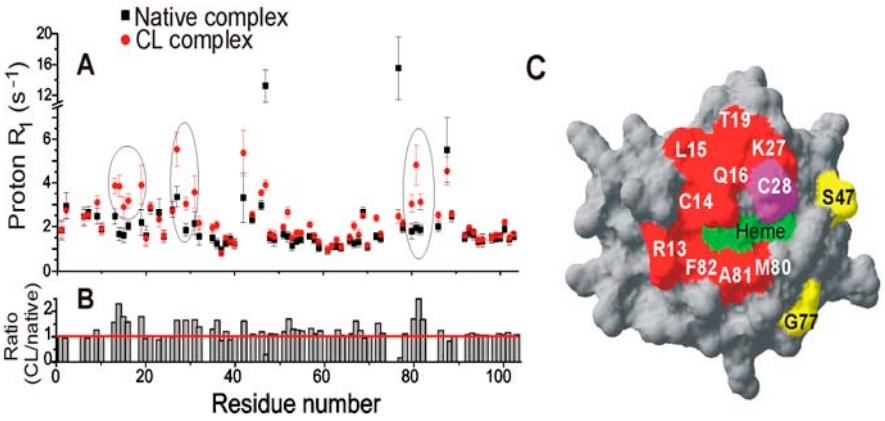

Figure 2.4. Paramagnetic relaxation enhancement. A) Amide proton R_1 values are plotted for observed C*c* residues for the native (black) and CL complex (red). B) The ratios of R_1 values (CL/native) are plotted for observed C*c* residues. C) Surface representation of C*c* with the site of cross-linking (C28) in magenta, residues with a R_1 ratio > 1.3 in red, and <0.5 in yellow and the heme in green.

control for the paramagnetic Adx is available to correct these effects. For this reason, the longitudinal relaxation rates (R_1) of amide protons were measured, for free C*c*, C*c* in the native complex and C*c* in the CL complex. The rates in the native complex state are only slightly larger than those in the free state.

Comparison of C*c* R_1 values in the native and CL complex indicates significant relaxation enhancement for some residues on C*c* when the orientation of the proteins has been fixed by cross-linking (Figure 2.4A and 2.4B). Surprisingly, two residues, S47 and G77, with large R_1 values in the free C*c* and the native complex, exhibit reduced relaxation rates in the CL complex. These residues are located close to the interaction interface but on one side of C28 (marked in yellow in Figure 2.4C) and are relatively far from the FeS cluster. A plausible explanation is that complex formation results in protection of these amide protons from solvent exchange, bringing the R_1 values into the usual range. All other affected residues are located close to the site of cross-linking (Figure 2.4C), suggesting that the relaxation enhancement is attributable to the proximity of the FeS cluster, as expected for a rigid complex. The absence of significant PREs in the native complex indicates that the average distance of all C*c* protons to the FeS cluster is too large to affect R_1, in accord with a dynamic nature of the complex.

Site specific spin labeling

To explore the interaction interface on Adx, a paramagnetic spin label, MTSL, was attached to C28 of the C*c* mutant and relaxation enhancement was measured for Adx amide protons in the native complex. C*c*V28C labeled with a diamagnetic control, MTS, was used to correct for all non-paramagnetic contributions to the transverse relaxation rate. The chemical shift perturbations observed for Adx upon complex formation with the control-labeled C*c* are very similar to those of the native complex formed by wild type (WT) C*c* and Adx, which indicates that the label does not interfere with the interaction between the proteins. In the complex with spin-labeled C*c*, many residues of Adx exhibit line broadening due to paramagnetic relaxation enhancement. The intensity (I) attenuation (I_{para}/I_{dia}) was used to calculate PREs, R_{2para} (Figure 2.5A). A map of intermolecular PREs onto the surface of Adx (Figure 2.5B) shows that the

residues with large R_{2para} (> 30 s^{-1}, red in Figure 2.5B) cover half of the surface area of Adx, without forming a single localized patch. The result indicates that within the native complex C*c* samples a large part of the surface of Adx.

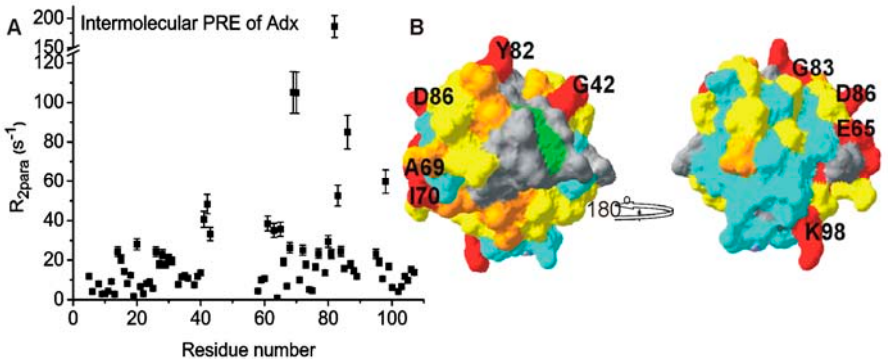

Figure 2.5. Spin labeling and intermolecular paramagnetic relaxation enhancement. A) Relaxation enhancement R_{2para} values are plotted for observed residues of Adx complexed with spin labeled C*c*. B) Surface representation of Adx, showing the residues affected by a spin label attached to C*c*V28C in the native complex. Residues are colored according to R_{2para} with ≥ 30, red; 20-30, orange; 11-20, yellow and <10 s^{-1}, light blue. Unobserved residues are in gray and the FeS binding loop in green.

Intermolecular pseudocontact shifts

Ferrous C*c* is diamagnetic while ferric C*c* carries a single unpaired electron, giving rise to pseudocontact shifts (PCS) of the surrounding nuclei. For most residues of C*c*, the difference in chemical shift between the oxidized and reduced state is dominated by the PCS. Upon complex formation, intermolecular PCS are expected also for Adx nuclei, as has been reported for example in the complex of cytochrome *f* and plastocyanin.[33] By comparison of the chemical shift changes observed for Adx binding to either ferrous or ferric C*c*, the PCS can be obtained, provided that the perturbations caused by binding are the same

in both redox states. In the native complex, the chemical shifts of Adx interacting with ferric and ferrous C*c* are very similar (Figure 2.6A), indicating the absence of significant intermolecular PCS. In contrast, in the CL complex, chemical shift differences are detected in some regions of Adx (Figure 2.6B). The shifts of the amides of residues D41-F43, I58-E60, F64 and T85-R89 show similar sizes (in ppm) and sign for amide proton and nitrogen dimensions, which is characteristic for PCS. The comparison of intermolecular PCS for native and CL complex suggests that the averaging of PCS in the native complex results from the interprotein dynamics.

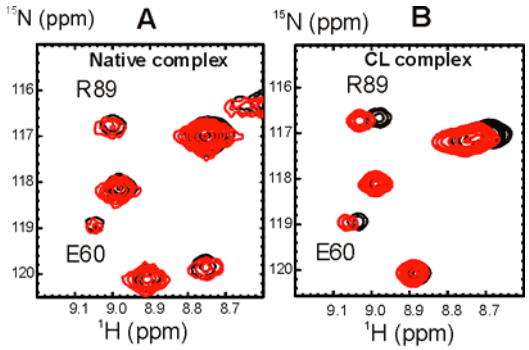

Figure 2.6. Intermolecular PCS detected on Adx for the native (A) and CL complex (B). Overlays of a region of the HSQC spectra of the complexes containing ^{15}N-Adx and reduced (red) or oxidized (black) C*c* are shown.

Pseudocontact shift simulations

The observation that Adx experiences intermolecular PCS from the heme in C*c* only in the CL but not in the native complex, strongly suggests that in the latter, such shifts are averaged by mobility of the Adx relative to C*c*. The size and sign of the PCS depends on both the metal-to-nucleus distance and the position of the nucleus within the frame of the magnetic susceptibility tensor, and thus reduction of the PCS can occur when Adx samples different orientations within the native complex. Simulations were carried out to determine the minimum

degree of mobility of Adx that is necessary to reduce the PCS to below the detection limit. Details are given in the materials and methods section. Figure

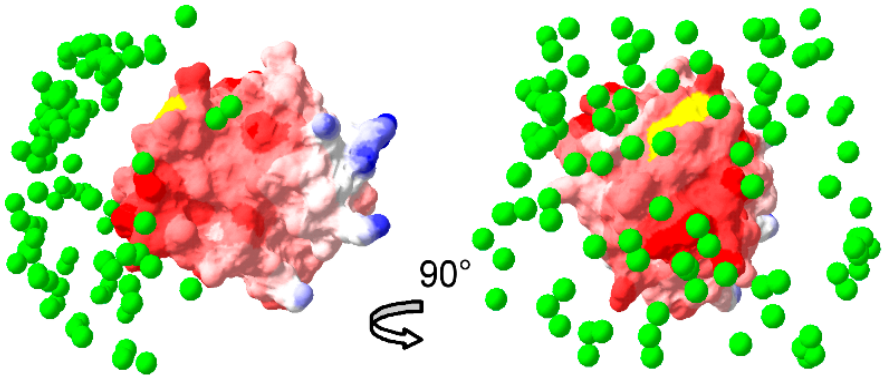

Figure 2.7. The ensemble of complex structures from the PCS simulation illustrates the degree of dynamics. Adx molecules are shown in surface representation colored according to the electrostatic potential with red, negative and blue, positive. The FeS binding loop is in yellow. The centers of mass of C*c* are represented by green spheres.

2.7 shows the result of the simulation. C*c* positions are represented by the centers of mass and illustrate the minimum mobility required in the native complex. Clearly, C*c* needs to sample a large area on Adx. This conclusion is in accord with the extensive chemical shift perturbation and PRE map observed for Adx in the native complex (Figures 2.3 and 2.4).

Structural modeling of CL complex

The PREs and PCSs observed in the CL complex were used to determine the relative orientations of C*c* and Adx. The model of the structure was derived by systematic search of the conformational space assuming rigid bodies for both proteins, with free rotation around the five torsion angles that link C*c*V28C C_α to AdxL80C C_α. The structures were scored on the basis of van der Waals, PCS and PRE energy terms. The final ensemble of 10 structures (Figure 2.8) has an

average RMSD of 1.7 Å from the mean for the Adx heavy atoms, after superposition of the C*c* molecules. The convergence of the structure model confirmed that the CL complex exists as a rigid complex. It shows that the contact surface for the CL complex contains part of the heme edge region of C*c* and the FeS loop and residues D72-Y82 of Adx. The interface in the calculated structure of the CL complex is consistent with the chemical shift mapping. The

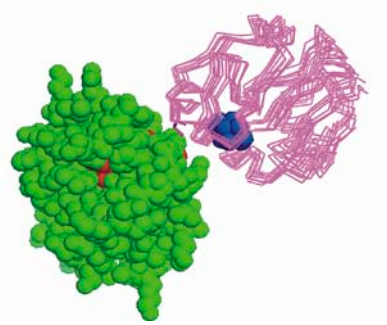

Figure 2.8. Structure of CL complex. The best ten structures (rmsd 1.7 Å) are shown with the C*c* molecule superimposed in spacefilling, green with heme in red, Adx as backbone trace in magenta and the FeS cluster in spacefilling, blue.

SAXS patterns computed from the ensemble of models display a good agreement with the experimental scattering from the CL complex in solution.

Discussion

The minimal model for protein complex formation consists of two steps. First, the proteins form an encounter complex, in which the partners can assume multiple orientations. Then, the final, well-defined and active complex is formed. The encounter state can be envisaged as a dynamic state, with one protein rolling over the surface of the other. Electrostatic forces are expected to dominate the interaction [(34)], due to their long-range effects, while desolvation of

the protein surface is probably limited. In the classical view, the encounter state exists only briefly and proceeds quickly to the final complex. However, evidence is accumulating that the encounter state may be populated significantly in weak protein complexes. Theoretical approaches, such as Brownian dynamics calculations on the electron transfer complex of cytochrome *c* peroxidase and C*c* suggested already decades ago that complexes can be partly of dynamic nature [(35)]. Experimental studies, such as fluorescence measurements on frozen solutions supported this view [(36)]. Over recent years, our NMR analyses demonstrated that the average chemical shift perturbations upon complex formation vary more than twenty fold among a range of electron transfer complexes.[(37)] It was proposed that the complexes which show large chemical shift perturbations are predominantly in a well-defined state, while those with overall small perturbations are dominated by the encounter state [(37,38)]. This idea is rationalized by the assumption that in the encounter state the proteins are still largely solvated, which means the chemical environment and thus the chemical shift of the amides are hardly perturbed. The CSP caused by any specific interactions that an amide experiences in a particular conformation is averaged with all other conformations of the encounter ensemble in which that amide has no specific interaction. Also this will reduce the observed CSP. Independently, kinetic studies also showed that some weak electron transfer complexes often should be represented by a dynamic ensemble, rather than a single complex [(5,39)]. The current study provides direct evidence that a protein complex can be truly dynamic, and thus can be considered to represent only the encounter complex. The very nature of this state makes it difficult to characterize, because of the dynamics and the absence of strong interactions. Therefore, a cross-linked counterpart of the complex was used for direct comparison. SAXS is a powerful method to probe the arrangement of domains in multiple domain complexes, protein oligomerization and complex formation and can provide the low resolution molecular envelope structure of proteins or protein complexes. A few

SAXS studies on redox complexes were reported previously, providing information complimentary to X-ray crystallography[40,41] and solution NMR studies [42]. Here, it was observed that only the native complex, not the CL complex exhibits oligomerization at low ionic strength and high protein concentration. The complexes do not associate directly into tetramers, oligomerization rather proceeds via trimers. Both observations suggest a stochastic way of association in support of a dynamic nature of the complex.

NMR CSPs were more localized and up to six-fold larger for Adx in the CL complex as compared to the native complex, in line with the observations for other complexes mentioned above. PCS from the heme onto Adx were observed in the CL complex, while being absent in the native complex. The correlation between a dynamic complex and the absence of intermolecular PCS was first proposed for the complex formed by plastocyanin and C*c*[2] and later also for other complexes [37,3,43]. Our simulations show that C*c* has to sample a large area on Adx to reduce the intermolecular PCS to insignificant values, which is in line with the large area of interaction identified by the chemical shift perturbations.

Similarly, the intermolecular PREs caused by the FeS cluster that can be observed for C*c* amides in the CL complex, are absent in the native complex. Relaxation effects depend on the sixth power of the distance between the FeS cluster and the observed amide proton and are relatively small because the cluster is buried within Adx. In the dynamic native complex the average distance between the amide protons of C*c* and the cluster is too large to result in PREs.

Recently, several studies showed that site-specific spin labeling combined with intermolecular PRE detection make it possible to obtain more information on low affinity, transient and dynamic protein-DNA or protein-protein complexs by NMR.[44,6,7,45] In our case, spin labeling on an exposed residue of C*c* close to the binding interface does result in PREs of many Adx amide protons. When the amide protons come sufficiently close to the spin label, even only for a small fraction of the time, they will exhibit enhanced relaxation. Therefore, this result

provides strong evidence that C*c* samples about 50% of the surface area of Adx. A comparison of the chemical shift perturbation maps with the electrostatic surface potential of Adx and C*c* (Figure. 2.3) clearly supports the notion that the encounter state is dominated by electrostatic forces. The interaction surface on Adc for C*c* comprise all four acidic patches (I-IV), while on C*c* the positively charged area around the heme edge is involved in the interaction. These findings are in line with our SAXS data as well as earlier crosslinking studies between horse C*c* and Adx, which showed that Arg13 (Lys14 in horse C*c*), Lys27, Lys72, and Lys79 are involved in the interaction with Adx.[46]. A docking study of horse C*c* and bovine Adx also supported this view [47].

Conclusions

In conclusion, all the data support the view that the complex between C*c* and Adx exists as a dynamic ensemble of orientations, without a dominant, well-defined form. Thus, this complex can be taken to represent a pure encounter complex. Such a model can be used to obtain better understanding of this elusive state of interacting proteins, yielding a more comprehensive picture of the process of complex formation.

Reference List

1. Delbrück M. and Adam G. 1968. Reduction of dimensionality biological diffusion processes. In Rich A. and Davidson N., Structural Chemistry and Molecular Biology: 198-215. San Francisco: Freeman.
2. Ubbink M. and Bendall D.S. (1997) Complex of plastocyanin and cytochrome c characterized by NMR chemical shift analysis. *Biochemistry* **36**: 6326-6335.
3. Worrall J.A.R., Reinle W., Bernhardt R., and Ubbink M. (2003) Transient protein interactions studied by NMR spectroscopy: The case of cytochrome *c* and adrenodoxin. *Biochemistry* **42**: 7068-7076.
4. Hoffman B.M., Celis L.M., Cull D.A., Patel A.D., Seifert J.L., Wheeler K.E., Wang J.Y., Yao J., Kurnikov I.V., and Nocek J.M. (2005) Differential influence of dynamic processes

on forward and reverse electron transfer across a protein-protein interface. *Proc.Natl.Acad.Sci.U.S.A.* **102**: 3564-3569.

5. Liang Z.X., Kurnikov I.V., Nocek J.M., Mauk A.G., Beratan D.N., and Hoffman B.M. (2004) Dynamic docking and electron-transfer between cytochrome b(5) and a suite of myoglobin surface-charge mutants. Introduction of a functional-docking algorithm for protein-protein complexes. *J.Am.Chem.Soc.* **126**: 2785-2798.
6. Tang C., Iwahara J., and Clore G.M. (2006) Visualization of transient encounter complexes in protein-protein association. *Nature* **444**: 383-386.
7. Volkov A.N., Worrall J.A.R., Holtzmann E., and Ubbink M. (2006) Solution structure and dynamics of the complex between cytochrome c and cytochrome c peroxidase determined by paramagnetic NMR. *Proc.Natl.Acad.Sci.U.S.A.* **103**: 18945-18950.
8. Grinberg A.V., Hannemann F., Schiffler B., Müller J., Heinemann U., and Bernhardt R. (2000) Adrenodoxin: Structure, stability, and electron transfer properties. *Proteins-Structure Function and Genetics* **40**: 590-612.
9. Lambeth J.D. and Kamin H. (1979) Adrenodoxin Reductase - Adrenodoxin Complex - Flavin to Iron-Sulfur Electron-Transfer As the Rate-Limiting Step in the Nadph-Cytochrome-C Reductase Reaction. *J.Biol.Chem.* **254**: 2766-2774.
10. Crowley P.B. and Ubbink M. (2003) Close encounters of the transient kind: Protein interactions in the photosynthetic redox chain investigated by NMR spectroscopy. *Acc.Chem.Res.* **36**: 723-730.
11. Uhlmann H., Kraft R., and Bernhardt R. (1994) C-Terminal Region of Adrenodoxin Affects Its Structural Integrity and Determines Differences in Its Electron-Transfer Function to Cytochrome-P-450. *J.Biol.Chem.* **269**: 22557-22564.
12. Rumbley J.N., Hoang L., and Englander S.W. (2002) Recombinant equine cytochrome c in Escherichia coli: High-level expression, characterization, and folding and assembly mutants. *Biochemistry* **41**: 13894-13901.
13. Roessle M.W., Klaering R., Ristau U., Robrahn B., Jahn D., Gehrmann T., Konarev P., Round A., Fiedler S., Hermes C., and Svergun D. (2007) Upgrade of the small-angle X-ray scattering beamline X33 at the European Molecular Biology Laboratory, Hamburg. *J.Appl.Crystallogr.* **40**: S190-S194.
14. Konarev P.V., Petoukhov M.V., Volkov V.V., and Svergun D.I. (2006) ATSAS 2.1, a program package for small-angle scattering data analysis. *J.Appl.Crystallogr.* **39**: 277-286.
15. Konarev P.V., Volkov V.V., Sokolova A.V., Koch M.H.J., and Svergun D.I. (2003) PRIMUS: a Windows PC-based system for small-angle scattering data analysis. *J.Appl.Crystallogr.* **36**: 1277-1282.
16. Svergun D.I. (1992) Determination of the Regularization Parameter in Indirect-Transform Methods Using Perceptual Criteria. *J.Appl.Crystallogr.* **25**: 495-503.
17. Porod, G 1982. In Glatter and Kratky,O., General theory. Small-angle X-ray scattering: 17-51. London: Academic Press.
18. Svergun D.I. (1999) Restoring low resolution structure of biological macromolecules from solution scattering using simulated annealing (vol 76, pg 2879, 1999). *Biophys.J.* **77**: 2896.
19. Svergun D., Barberato C., and Koch M.H.J. (1995) CRYSOL - A program to evaluate x-ray solution scattering of biological macromolecules from atomic coordinates. *J.Appl.Crystallogr.* **28**: 768-773.
20. Petoukhov M.V. and Svergun D.I. (2005) Global rigid body modeling of macromolecular complexes against small-angle scattering data. *Biophys.J.* **89**: 1237-1250.
21. Berghuis A.M. and Brayer G.D. (1992) Oxidation State-Dependent Conformational-Changes in Cytochrome-C. *J.Mol.Biol.* **223**: 959-976.
22. Müller A., Müller J., Müller Y., Uhlman, H., Bernhard, R., and Heineman (1998) New aspects of electron transfer revealed by the crystal structure of a truncated bovine adrenodoxin, Adx(4-108). *Structure* **6**: 269-280.

23. Worrall J.A.R., Kolczak U., Canters G.W., and Ubbink M. (2001) Interaction of yeast iso-1-cytochrome c with cytochrome c peroxidase investigated by [N-15,H-1] heteronuclear NMR spectroscopy. *Biochemistry* **40**: 7069-7076.
24. Helgstrand M., Kraulis P., Allard P., and Härd T. (2000) Ansig for Windows: An interactive computer program for semiautomatic assignment of protein NMR spectra. *J.Biomol.NMR* **18**: 329-336.
25. Vlasie M.D., Fernandez-Busnadiego R., Prudêncio M., and Ubbink M. (2008) Conformation of Pseudoazurin in the 152 kDa Electron Transfer Complex with Nitrite Reductase Determined by Paramagnetic NMR. *J.Mol.Biol.* **375**: 1405-1415.
26. Niccolai N., Spiga O., Bernini A., Scarselli M., Ciutti A., Fiaschi I., Chiellini S., Molinari H., and Temussi P.A. (2003) NMR studies of protein hydration and TEMPOL accessibility. *J.Mol.Biol.* **332**: 437-447.
27. Deschamps M.L., Pilka E.S., Potts J.R., Campbell I.D., and Boyd J. (2005) Probing protein-peptide binding surfaces using charged stable free radicals and transverse paramagnetic relaxation enhancement (PRE). *J.Biomol.NMR* **31**: 155-160.
28. Louie G.V. and Brayer G.D. (1990) High-Resolution Refinement of Yeast Iso-1-Cytochrome-C and Comparisons with Other Eukaryotic Cytochromes-C. *J.Mol.Biol.* **214**: 527-555.
29. Guex N. and Peitsch M.C. (1997) SWISS-MODEL and the Swiss-PdbViewer: An environment for comparative protein modeling. *Electrophoresis* **18**: 2714-2723.
30. Schwieters C.D., Kuszewski J.J., Tjandra N., and Clore G.M. (2003) The Xplor-NIH NMR molecular structure determination package. *J.Magn.Reson.* **160**: 65-73.
31. Beilke D., Weiss R., Lohr F., Pristovsek P., Hannemann F., Bernhardt R., and Rüterjans H. (2002) A new electron transport mechanism in mitochondrial steroid hydroxylase systems based on structural changes upon the reduction of adrenodoxin. *Biochemistry* **41**: 7969-7978.
32. Petersen M.T.N., Jonson P.H., and Petersen S.B. (1999) Amino acid neighbours and detailed conformational analysis of cysteines in proteins. *Protein Eng.* **12**: 535-548.
33. Ubbink M., Ejdebäck M., Karlsson B.G., and Bendall D.S. (1998) The structure of the complex of plastocyanin and cytochrome *f*, determined by paramagnetic NMR and restrained rigid-body molecular dynamics. *Structure* **6**: 323-335.
34. Suh J.Y., Tang C., and Clore G.M. (2007) Role of electrostatic interactions in transient encounter complexes in protein-protein association investigated by paramagnetic relaxation enhancement. *J.Am.Chem.Soc.* **129**: 12954-12955.
35. Northrup S.H., Boles J.O., and Reynolds J.C.L. (1988) Brownian Dynamics of Cytochrome-C and Cytochrome-C Peroxidase Association. *Science* **241**: 67-70.
36. McLendon G., Zhang Q., Wallin S.A., Miller R.M., Billstone V., Spears K.G., and Hoffman B.M. (1993) Thermodynamic and Kinetic Aspects of Binding and Recognition in the Cytochrome-C Cytochrome-C Peroxidase Complex. *J.Am.Chem.Soc.* **115**: 3665-3669.
37. Worrall J.A.R., Liu Y.J., Crowley P.B., Nocek J.M., Hoffman B.M., and Ubbink M. (2002) Myoglobin and cytochrome b(5): A nuclear magnetic resonance study of a highly dynamic protein complex. *Biochemistry* **41**: 11721-11730.
38. Prudêncio M. and Ubbink M. (2004) Transient complexes of redox proteins: structural and dynamic details from NMR studies. *J.Mol.Recognit.* **17**: 524-539.
39. Furukawa Y., Matsuda F., Ishimori K., and Morishima I. (2002) Investigation of the electron-transfer mechanism by cross-linking between Zn-substituted myoglobin and cytochrome b(5). *J.Am.Chem.Soc.* **124**: 4008-4019.
40. Jones M., Basran J., Sutcliffe M.J., Grossmann J.G., and Scrutton N.S. (2000) X-ray scattering studies of Methylophilus methylotrophus (sp W(3)A(1)) electron-transferring flavoprotein - Evidence for multiple conformational states and an induced fit mechanism for assembly with trimethylamine dehydrogenase. *J.Biol.Chem.* **275**: 21349-21354.

41. Leys D., Basran J., Talfournier F., Sutcliffe M.J., and Scrutton N.S. (2003) Extensive conformational sampling in a ternary electron transfer complex. *Nat.Struct.Biol.* **10**: 219-225.
42. Perry A., Tambyrajah W., Grossmann J.G., Lian L.Y., and Scrutton N.S. (2004) Solution structure of the two-iron rubredoxin of Pseudomonas oleovorans determined by NMR spectroscopy and solution X-ray scattering and interactions with rubredoxin reductase. *Biochemistry* **43**: 3167-3182.
43. Volkov A.N., Ferrari D., Worrall J.A.R., Bonvin A.M.J.J., and Ubbink M. (2005) The orientations of cytochrome c in the highly dynamic complex with cytochrome b(5) visualized by NMR and docking using HADDOCK. *Protein Sci.* **14**: 799-811.
44. Iwahara J. and Clore G.M. (2006) Detecting transient intermediates in macromolecular binding by paramagnetic NMR. *Nature* **440**: 1227-1230.
45. Blundell T.L. and Fernandez-Recio J. (2006) Cell biology - Brief encounters bolster contacts. *Nature* **444**: 279-280.
46. Geren L.M. and Millett F. (1981) Interaction Between Adrenodoxin and Cytochrome-C. *J.Biol.Chem.* **256**: 4851-4855.
47. Müller J.J., Lapko A., Ruckpaul K., and Heinemann U. (2003) Modeling of electrostatic recognition processes in the mammalian mitochondrial steroid hydroxylase system. *Biophys.Chem.* **100**: 281-292.